



Production of silica-based ceramics sintered under nitrogen atmosphere from rice husk and sugarcane bagasse ash

Wiphawan KHOPHONG and Benya CHERDHIRUNKORN*

Faculty of Science and Technology, Thammasat University, Phahonyothin road, Klong Luang, Pathum Thani, 12120, Thailand

*Corresponding author e-mail: benya@tu.ac.th

Received date:
30 September 2019
Revised date:
24 March 2020
Accepted date:
6 April 2020

Keywords:
Nitride silica-based ceramics
Rice husk ash
Sugarcane bagasse ash
Nitridation

Abstract

Nitride silica-based ceramics were prepared by sintering under nitrogen atmosphere using rice husk ash and bagasse ash as raw materials. X-ray Fluorescence Spectrometry (XRF) and X-ray Diffractometer (XRD) studies revealed that the main phase of rice husk ash (after calcined at 600°C for 6 h.) was amorphous silica, whereas the sugarcane bagasse ash contained quartz and CaCO₃. Thus, both ashes would be a good source for silica. Two batches of the 100 wt% rice husk ash (RHA100) and the mixture of 50 wt% rice husk ash and 50 wt% bagasse ash (RHA50BA50) were wet milled using planetary ball milling machine, and were then dried at 90°C. The powders were uniaxially pressed at the pressure of 150 MPa. The disk shape samples were sintered at 1300-1500°C in the nitrogen atmosphere with gas flow rate of 600 ml/min. The physical and mechanical properties of the sintered disk shape samples were determined. The phase structure and microstructure of the samples were investigated using XRD and SEM techniques, respectively. The main phases obtained after sintering were cristobalite, tridymite, α and β -silicon nitride and SiC. The RHA50BA50 sample sintered at 1450°C showed the optimum properties with low firing shrinkage, low water absorption and high strength.

1. Introduction

Rice and sugarcane are major agricultural crops of Thailand, producing rice husk and sugarcane bagasse as byproducts. These can be used as biofuel in power plants. Rice husk ash (RHA) and sugarcane bagasse ash (BA) are left after combustion, and they are rich of silica and carbon. Although these can be used for soil modification in agricultural applications, abundant quantities remain. RHA is an attractive waste material as it has high silica content (93-97% for acid treated RHA) [1]. BA is also high in silica (60-70%) and also contains high calcium [2]. The extraction of silica from other agricultural wastes, such as bamboo leaf and groundnut shell has also been interested [2]. Thus, RHA and BA are alternative sources of silica, with applications in glass, tile, brick, refractory making, engine components, metal cutting, and crucibles [3-7].

The production of silicon-based ceramics, such as Si₃N₄, SIALON, SiC, and their composite, has been attracting attention from researchers due to their high strength and thermal stability. One well-known method of silicon nitride (Si₃N₄) production involves direct reaction between silicon (Si) and nitrogen (N₂): 3Si(s) + 2N₂(g) → Si₃N₄(s) [8]. SiC can be produced by the Acheson process, using carbothermal reduction of silica by carbon in an electric arc furnace. However, the cost of the raw materials and production is quite high. Thus, alternative methods and techniques have been proposed to produce nitride silica-based ceramics from cheaper raw materials such as rice husk or bamboo

leaf [9-13]. Several studies have reported the production of high purity silica from RHA treated with acid prior to high temperature calcination. [12,14,15] A composite of SiC and Si₃N₄ was obtained by carbothermal reduction of rice husk under a nitrogen and argon atmosphere at 1450°C. [12]

High purity silica [2,14] and non-oxide nitride silica-based ceramics [16] including, SiC [17] and SiC/Si₃N₄ composite [12], have been produced from rice husk. The use of BA in ceramic applications has also been reported, producing cement [18], aggregate for concrete [19], floor tiles [20], and silica nanoparticles [21]. However, the use of BA or mixtures of RHA and BA, has not been intensively studied for production of nitride silica-based ceramics. One such technique involves sintering under a nitrogen atmosphere. The present work used an uncomplicated method to fabricate nitride silica-based ceramics from RHA and BA. Mixed phases of oxide and nitride silica-based ceramics were expected. The physical and mechanical properties, phase structure, and microstructure were investigated.

2. Experiment procedure

2.1 Materials

Ceramics were prepared using RHA and BA as main raw materials. The available rice husk (from a rice paddy production in Nakornpatom province, Thailand) and BA (from a biomass power plant, Lopburi,

Thailand) were calcined in the oxidation atmosphere at 600°C for 6 h using an electric furnace. The calcination greatly influence the decomposition of organic matter the rice husk and BA. The chemical composition and phase structure of these calcined materials were obtained using XRF (Bruker, S8 TIGER) and XRD (PANalytical, X'pert Pro), respectively. The microstructures were observed using SEM (Hitachi, S-3400N Type II)

2.2 Fabrication by sintering under nitrogen atmosphere

Two test samples were prepared: calcined rice husk (RHA100) and a mixture of RHA and BA at 50:50 by weight (RHA50BA50). These were planetary ball milled (Fritsch Pulverisette 5) using water as a medium for 1 h at a rotational speed of 200 rpm. Polyvinyl alcohol (3 wt% PVA) and polyethylene glycol (1 wt% PEG) were used as a binder and a lubricant, respectively. The milled slurry was oven dried at 90°C. The resulting powders were sieved through mesh#200 (75 µm), and were then uniaxially pressed into a die with a diameter of 13 mm at 150 MPa. The disk-shaped samples were sintered in an alumina tube furnace at a heating rate of 5°C·min⁻¹ to 1300, 1350, 1400, 1450 and 1500°C.

Nitrogen gas (99%) was flowed at 600 ml·min⁻¹ to create a nitrogen atmosphere. Sample preparation is shown as Figure 1.

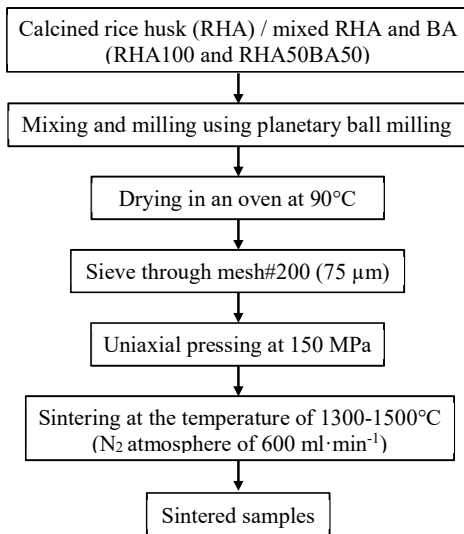


Figure 1. Preparation of nitride silica-based ceramics via direct nitridation).

2.3 Characterization of the sintered samples

After sintering, the bulk density, apparent density, apparent porosity (%), and water absorption (%) of the RHA100 and RHA50BA50 samples were determined using Archimedes principle (ASTM standard C20). The firing shrinkage of the samples was measured

following ASTM C326-09 [22]. The thermal conductivity of the samples sintered at 1450°C was measured using a Thermal Constant Analyzer (Hot Disk TCA).

The indirect tensile strength (Brazilian test) (Figure 2) was determined using a universal testing machine (Tinius Olsen, H50KS). The test was carried out at the compression rate of 5 mm/min. The indirect tensile yield strength was calculated according to equation (1).

$$ITS = 2P/\pi DT \quad (1)$$

where ITS is indirect tensile yield strength
 P is the applied load
 D is the disk diameter
 T is the sample thickness

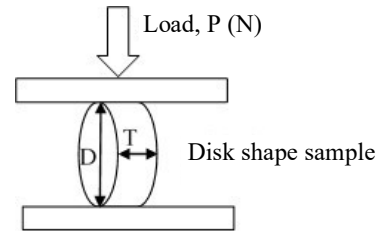


Figure 2. Schematic of Brazilian test for tensile strength.

The compressive strength and modulus of rupture (MOR) of the 1450°C samples were also measured using the universal testing machine.

The phase structures of samples were investigated using XRD (BRUKER, D8 Discover series 2) using Cu K_α (λ=1.5406 Å). The measurements were obtained at 2θ of 10° to 80° with the step size of 0.02° and the step time of 2 s. Samples sintered at 1500°C were excluded because they partly melted. The microstructure and elemental composition of the 1450°C samples were analyzed using SEM and EDS (JEOL model JSM-6480LV).

3. Results and discussion

3.1 Chemical compositions, phase structures and microstructures of RHA and BA

Table 1 shows the chemical composition of the calcined RHA and BA, determined by XRF. The RHA comprised 93.7 wt% silica. The BA comprised 57.6 wt% silica and 12.4 wt% calcium oxide. The XRD pattern shown in Figure 3 suggested that the major phase of the RHA was amorphous silica, as a broad peak was observed at a 2θ scattering angle of 15 to 30°. The major phases of the calcined BA were quartz (SiO₂), calcite (CaCO₃), and potassium oxide (K₂O), as shown in Figure 4. Since both RHA and BA contained significant silica, they provide a potential alternative source for the fabrication of nitride silica-based material. SEM images of the RHA and BA particles (Figure 5) showed a rough and porous surface, which should enhance the nitridation reaction.

Table 1. Chemical composition of RHA and BA calcined at 600°C for 6 h.

Chemical composition	Calcined RHA (wt%)	Calcined BA (wt%)
SiO ₂	93.7	57.6
CaO	0.57	12.4
Al ₂ O ₃	-	4.61
K ₂ O	1.43	4.11
MgO	0.21	2.73
Fe ₂ O ₃	445 ppm	2.63
P ₂ O ₅	0.44	1.55
SO ₃	0.18	0.98
Na ₂ O	882 ppm	0.38
TiO ₂	-	0.3

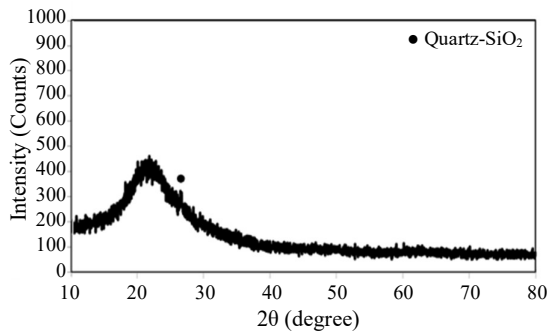


Figure 3. XRD pattern of RHA calcined at 600°C.

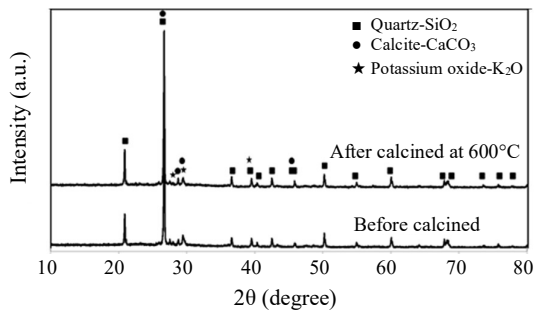


Figure 4. XRD patterns of BA (before and after calcination).

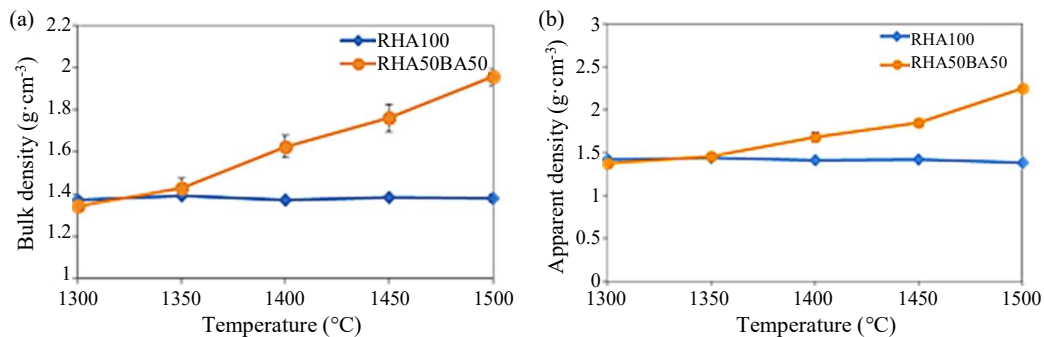


Figure 6. Plots of (a) bulk density, (b) apparent density, (c) water absorption (%), (d) porosity (%) and (e) firing shrinkage (%) as a function of sintering temperature for RHA100 and RHA50BA50 samples.

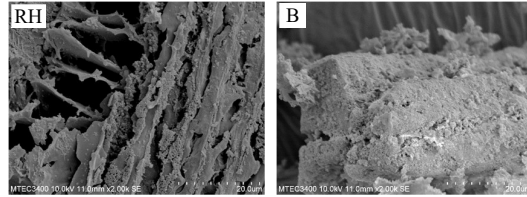


Figure 5. SEM images of RHA and BA calcined at 600°C.

3.2 Characterization of sintered samples

3.2.1 Physical properties

As can be seen from Figure 6 (a) and (b), the bulk density and apparent density of the RHA50BA50 sample increased as the sintered temperature was increased from 1300 to 1500°C, whereas those of RHA100 were lower and remained constant. The water absorption and porosity (%) of RHA50BA50 markedly reduced as the sintering temperature increased, whereas the water absorption of RHA100 slightly increased (Figure 6 (c) and (d)). Figure 6 (e) shows that the firing shrinkage of the RHA50BA50 samples increased as the sintering temperature increased. The addition of BA may encourage densification during sintering through pore reduction. At 1500°C, distortion was observed in the RHA50BA50 sample. Its high Ca content may induce a glassy phase, as Ca normally acts as flux, which may lower the melting point.

3.2.2 Thermal conductivity

For samples sintered at 1450°C, the thermal conductivity of RHA100 was 0.7785 W·mK⁻¹ and that of RHA50BA50 was 0.5774 W·mK⁻¹. From the previous results, the RHA50BA50 sample had a higher bulk density and lower water absorption, while the thermal conductivity was lower, suggesting that another mechanism may account for the low thermal conductivity.

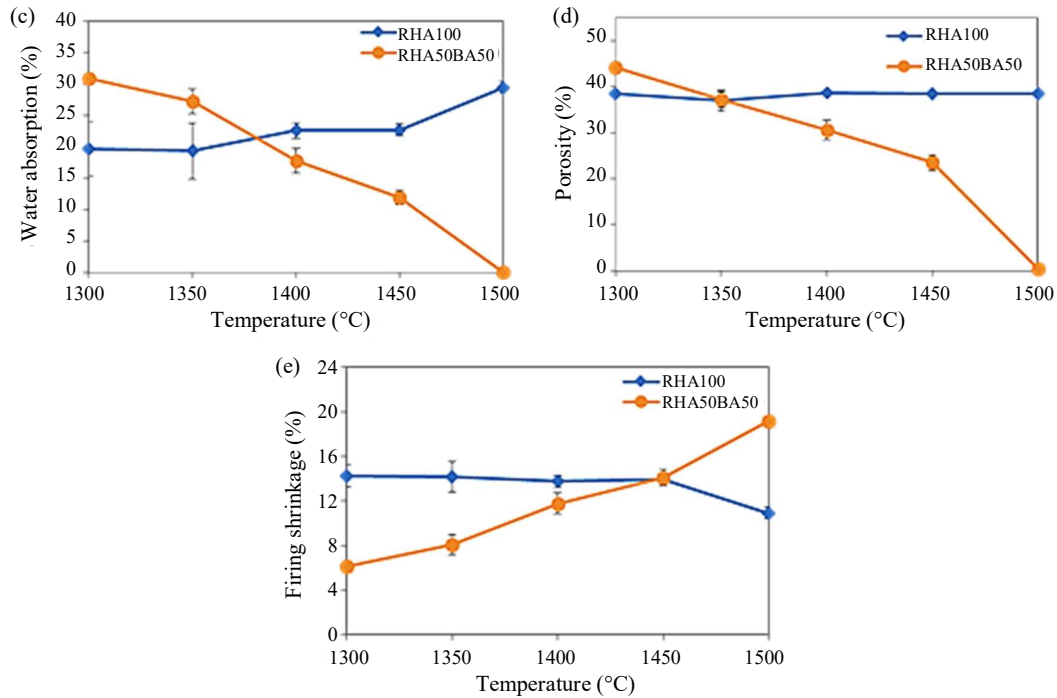


Figure 6. Plots of (a) bulk density, (b) apparent density, (c) water absorption (%), (d) porosity (%) and (e) firing shrinkage (%) as a function of sintering temperature for RHA100 and RHA50BA50 samples. (continue)

3.2.3 Mechanical properties

The indirect tensile strength of sintered samples is shown in Figure 7. The strength of the RHA100 samples decreased as the sintering temperature increased beyond 1350°C. The highest strength was observed for the RHA50BA50 sample sintered at 1500°C in a nitrogen atmosphere. As shown in Figure 6 (a) and (c), this sample had the highest density and lowest water absorption. However, a sintering temperature of 1500°C is not optimal since distortion took place. The optimum sintering temperature for all samples in this study was 1450°C.

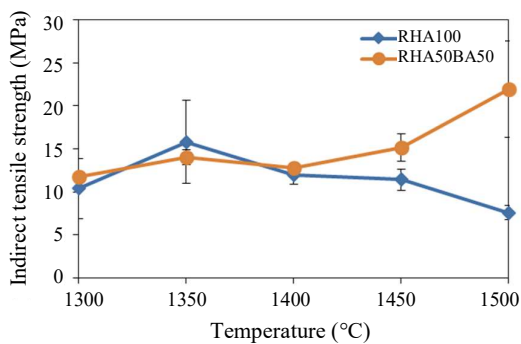


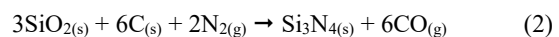
Figure 7. Plots of the indirect tensile strength as a function of the sintering temperature for the RHA100 and RHA50BA50 samples.

The compressive strength of the RHA100 and RHA50BA50 samples sintered at 1450°C were 50.30

and 50.15 MPa, respectively, and the modulus of rupture (MOR) were 13.08 and 36.84 MPa. However, the MOR of RHA50BA50 was higher than that of RHA100. The MOR results were similar to the indirect tensile strength.

3.2.4 Phase structures of sintered samples

The XRD patterns of the 1300 to 1450°C samples are shown in Figures 8 and 9. The major phases observed were cristobalite, tridymite, SiC, α -Si₃N₄ and β -Si₃N₄. Cristobalite was the major phase at the temperature of 1300°C. As the temperature increased, the tridymite peak intensity increased in both RHA100 and RHA50BA50 samples. However, in the RHA50BA50 sample, the cristobalite peak reduced as the temperature increased, so that tridymite dominated at 1450°C. In the RHA100 sample, no decline in the cristobalite peak was observed. This could be the effect of calcium (Ca) and potassium (K) (alkali ions) presented in the sugarcane bagasse ash, which agree with the work of Shinohara [1], where the present of 3% K₂O in the RHA sample showed the dominant of tridymite phase above 1000°C. In addition, the minor phase of Si₃N₄ was observed in both samples as SiO₂ may reacted with C from the remained organic matter after the calcination of the raw materials, and N₂ gas. The reaction mechanism of this transformation is described by the following reaction equation (2). [8]



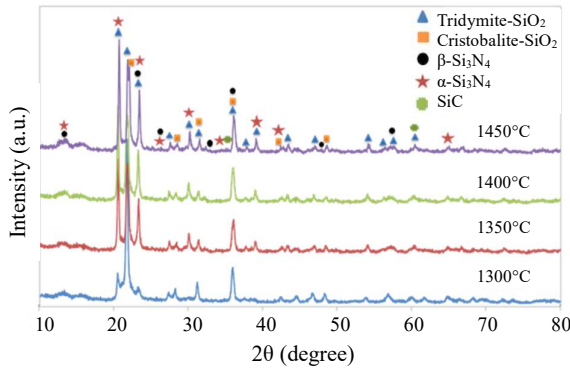


Figure 8. XRD patterns of RHA100 sintered at 1300-1450°C.

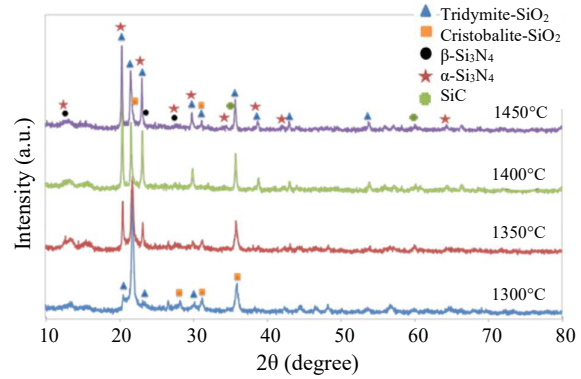


Figure 9. XRD patterns of RHA50BA50 sintered at 1300-1450°C.

3.2.5 SEM and EDS analysis of sintered samples

Figure 10 shows SEM images with their corresponding EDS attached for the polished and acid etched 1450°C RHA100 and RHA50BA50 samples. Higher porosity was observed in RHA100 sample agreeing with the physical properties shown in Figure 6. This may also related to the mechanical properties as reported in section 3.2.3. The lower strength in RHA100 may be due to higher porosity. There were two major phases present in the SEM image of RHA100 sample, whereas at least three phases were observed in RHA50BA50 samples. Although the nitride phases were not clearly observed in XRD results for both RHA100 and RHA50BA50 samples,

the EDS analysis revealed that there were Si, N, O, C, Ca and K in the RHA 100 samples and Si, N, O, C, Ca and Al in RHA50BA50 samples, indicating the present of nitride phase in these samples (9-10 wt% of nitrogen). In RHA100, two phases were the lighter grey phase containing Si, O, Ca, K and N, and the dark grey phase containing Si, O and C. For the RHA50BA50 sample, the distribution of small closed pores was obviously seen throughout the lighter grey phase (spot 2). The EDS analysis indicated that this phase contained high Ca (16.5 wt%), which would be the phase derived from the bagasse ash. The small closed pore may give rise to the lower thermal conductivity of this sample as reported in section 3.2.2.

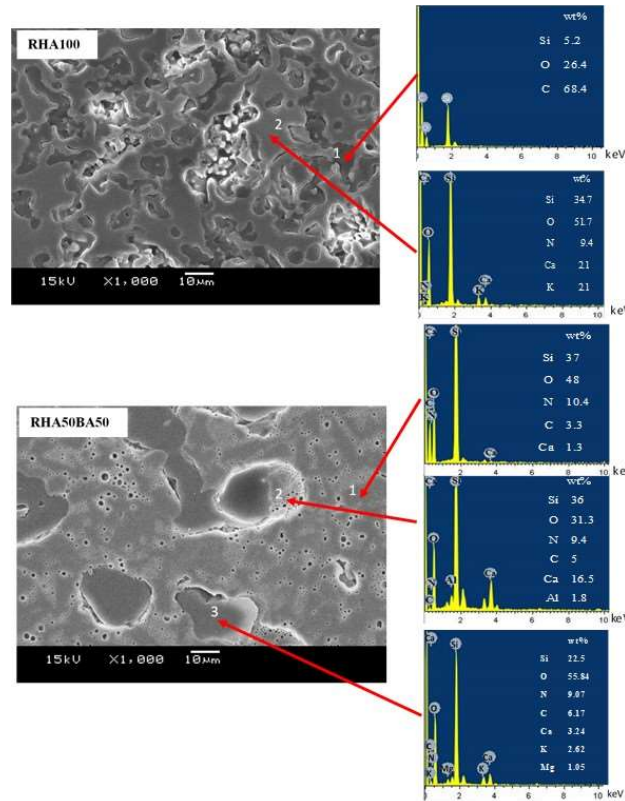


Figure 10. SEM images of RHA100 and RHA50BA50 at 1450°C and EDS analysis.

4. Conclusions

1. The feasibility of producing nitride silica-based ceramic from rice husk and sugarcane bagasse ash was studied by sintering in nitrogen atmosphere. XRD results suggested that the mixed phases obtained after sintering consisted of cristobalite, tridymite, α - Si_3N_4 , β - Si_3N_4 , and SiC. The EDS analysis confirmed the present of nitrogen in both RHA100 and RHA50BA50 samples.

2. Although the common form of the crystalline silica in the high temperature (1470-1727°C) treated materials is cristobalite. The present of Ca and K ions in BA may stabilize tridymite phase in RHA50BA50 sample sintered at the temperature above 1400°C.

3. The addition of the bagasse ash (RHA50BA50 sample) encouraged the densification in nitride silica-based ceramics, and provided the better properties for the sample sintered at 1450°C.

4. The optimum sintering temperature for both RHA100 and RHA50BA50 samples was 1450°C. Although the higher strength was obtained at the sintering temperature of 1500°C, the sample distortion occurred.

5. Acknowledgements

This work is supported by the National Research Council of Thailand (NRCT), Grant No.11/2561, and Graduate Grant No. 05/2562. Faculty of Science and Technology Thammasat University and Scholarship for talent student to study graduate program in Faculty of Science and Technology Thammasat University, Contract No. 18/2560. In addition, we would also like to thank National Metal and Materials Science Center (MTEC) and Materials Science Chulalongkorn University for their supports.

References

[1] Y. Shinohara and N. Kohyama, "Quantitative analysis of tridymite and cristobalite crystallized in rice husk ash by heating," *Industrial Health*, vol. 42 (2), pp. 277-285, 2004.

[2] V. Vaibhav, U. Vijayalakshmi, and S. M. Roopan, "Agricultural waste as a source for the production of silica nanoparticles," *Spectrochimica Acta Part A: Molecular and Biomolecular Spectroscopy*, vol. 139, pp. 515-520, 2015.

[3] S. Hampshire, "Silicon Nitride ceramics-review of structure, processing and properties," *Journal of Achievements in Materials and Manufacturing Engineering*, vol. 24 (1), pp. 43-60, 2007.

[4] S. Somiya, M. Mitomo, and M. Yoshimura, Eds., *Silicon Nitride-1*, London, U.K.: Ceramics Applied Science, 1990.

[5] S. K. S. Hossin, L. Mathur, and P. K. Roy, "Rice husk/rice husk ash as an alternative

source of silica in ceramics: A review," *Journal of Asian Ceramic Societies*, vol. 6 (4), pp. 299-313, 2018.

[6] V. P. Della, I. Kuhn, and D. Hotza, "Rice husk ash as an alternate source for active silica production," *Materials Letters*, vol. 57, pp. 818-821, 2002.

[7] K. C. P. Faria, R. F. Gurgel, and J. N. F. Holanda, "Recycling of sugarcane bagasse ash waste in the production of clay bricks," *Journal of Environmental Management*, vol. 101, pp. 7-12, 2012.

[8] H. Arik, "Synthesis of Si_3N_4 by the carbothermal reduction and nitridation of diatomite," *Journal of the European Ceramic Society*, vol. 23, pp. 2005-2014, 2003.

[9] F. Wang, X. Qin, G. Jin, and X. Guo, "Temperature-controlled synthesis of Si_3N_4 nanomaterials via direct nitridation of Si powders," *Physica E ScienceDirect*, vol. 42, pp. 2033-2035, 2010.

[10] A. O. Kurt, and T. Davies, "Synthesis of Si_3N_4 using sepiolite and various sources of carbon," *Journal of Materials Science*, vol. 36, pp. 5895-5901, 2001.

[11] T. H. Liou and F. W. Chang, "The nitridation kinetics of pyrolyzed rice husk," *Industrial & Engineering Chemistry Research*, vol. 35, pp. 3375-3383, 1996.

[12] C. Real, J. M. Cordoba, and M. D. Alcala, "Synthesis and characterization of SiC/ Si_3N_4 composites from rice husks," *Ceramics International*, vol. 44, pp. 14645-14651, 2018.

[13] A. A. Adediran, K. K. Alaneme, I. O. Oladele, and E. T. Akinlabi, "Processing and structural characterization of Si-based carbothermal derivatives of bamboo leaf," *Procedia Manufacturing*, vol. 35, pp 389-394, 2019.

[14] R. A. Bakar, R. Yahya, and S.N. Gan, "Production of high purity amorphous silica from rice husk," *Procedia Chemistry*, vol. 19, pp. 189-195, 2016.

[15] J. Chun, Y. M. Gu, J. Hwang, K. K. Oh, and J. H. Lee, "Synthesis of ordered mesoporous silica with various pore structures using high-purity silica extracted from rice husk," *Journal of Industrial and Engineering Chemistry*, vol. 81, pp. 135-143, 2020.

[16] N. Soltani, A. Bahrami, M. I. Pech-Canul, L. A. González, "Review on the physicochemical treatments of rice husk for production of advanced materials," *Chemical Engineering Journal*, vol. 264, pp. 899-935, 2015.

[17] S. T. Alweendo, O. T. Johnson, M. B. Shongwe, F. P. L. Kavishe, and J. O. Borode, "Synthesis, Optimization and Characterization of Silicon Carbide (SiC) from Rice Husk," *Procedia Manufacturing*, vol. 35, pp. 962-967, 2019.

- [18] D.-H. Le and Y.-N. Sheen, "My Ngoc-Tra Lam, Fresh and hardened properties of self-compacting concrete with sugarcane bagasse ash-slag blended cement," *Construction and Building Materials*, vol. 185, pp. 138-147, 2018.
- [19] G. P. Lyra, V. dos Santos, B. C. de Santis, R. R. Rivaben, C. Fischer, E. M. de J. A. Pallone, and J. A. Rossignolo, "Reuse of sugarcane bagasse ash to produce a lightweight aggregate using microwave oven sintering," *Construction and Building Materials*, vol. 222, pp.222-228, 2019.
- [20] M. A. S. Schettino, F. B. Siqueira, and J. N. F. Holanda, "Densification behavior of floor tiles added with sugarcane bagasse ash waste," *Ciência & Tecnologia dos Materiais*, vol. 28 (1), pp. 60-66, 2016.
- [21] G. Falk, G. P. Shinhe, L. B. Teixeira, E. G. Moraes, and A. P. Novaes de Oliveira, "Synthesis of silica nanoparticles from sugarcane bagasse ash and nano-silicon via magnesiothermic reactions," *Ceramics International*, vol. 45 (17), pp. 21618-21624, 2019.
- [22] American Society for testing and Material, "ASTM Designation C20-00, C326: General Product, Chemical Specialties, and End Use Products," in *Annual book of ASTM Standards*, USA: ASTM International, pp. 6-9, 2005.